Capacitor-less Photovoltaic (PV) Cell-Level Power Balancing using Diffusion Charge Redistribution

Arthur H. Chang, Al-Thaddeus Avestruz, and Steven B. Leeb
Department of Electrical Engineering and Computer Science
Massachusetts Institute of Technology
Cambridge, MA, USA
Email: arthurhc@mit.edu

***Abstract*—This paper presents a new strategy, *diffusion charge redistribution (DCR)*, for balancing power among photovoltaic cells to increase energy extraction and to improve maximum power point tracking (MPPT) efficiency under partial shading conditions. With DCR, testing and binning during cell manufacturing can be eliminated, and significant cost savings can be achieved during production. The proposed technique performs power balancing by taking advantage the intrinsic diffusion capacitance of the solar cells and requires no external passive components for energy storage, thereby minimizing power electronics cost and complexity. Strings balanced by this technique exhibit power versus current curves that are convex, which also greatly reduces the cost and complexity of the required MPPT algorithm.**

I. Introduction

Photovoltaic (PV) power modules are traditionally configured as a string of solar cells [20]. In this series-connected configuration, the overall string current is limited by the available current of the lowest-performing solar cell in the string. Therefore, external operating conditions such as partial shading and dirt accumulation can severely limit the available power from the string, even if only a few cells are affected out of a large string [1-8].

Bypass diodes in parallel with sub-strings can mitigate this problem. This approach enables the higher-performing cells to output higher currents, bypassing lower-performing sub-strings altogether, potentially extracting more power from the string. However, any possible power generation from the lower performing cells is completely forgone and additional losses are also incurred from the bypass diodes. Furthermore, this results in an output power characteristic curve that is non-convex, which complicates maximum power point tracking (MPPT) algorithms [2,4].

Modular architectures such as cascaded dc-dc converters with a central inverter, micro-inverters, and their sub-module variants, have been proposed to allow local MPPT through distributed control [7-9]. However, their operation requires the processing of the full power from each PV element, which is a major disadvantage in terms of insertion loss. In addition, it is impractical to scale these approaches down to the cell-level, as per-cell inductors and capacitor banks may be required.

Recently, there has been a push towards differential power processing to balance mismatches in a PV string [1-6]. By only processing the mismatch power instead of the full power, significant reduction in power loss due to conversion efficiency and in power electronics size can be achieved, and many different architectures based on this principle have been proposed [1-6]. Most of these approaches also rely on the availability of external energy storage elements. For example, the sub-module integrated converter in [1] employs flyback converters which require a discrete transformer per PV element as energy storage. In the PV-to-PV differential architecture proposed in [4,5], buck-boost converters with external inductors are used between adjacent PV elements. Lastly, discrete capacitors are needed in parallel with each PV sub-module and in between adjacent PV sub-modules in the resonant switched-capacitor converter proposed in [2,3].

This paper explores the concept of differential power processing applied at the cell-level, while making the tradeoff of eliminating the requirement of external passive component for intermediate energy storage. The proposed technique makes use of the intrinsic diffusion capacitance of the solar cells as the main energy storage element, at the cost of processing part of the common-mode generated power. This technique is termed *diffusion charge redistribution (DCR)*. Theoretical background for quantifying the solar cell diffusion capacitance is presented along with experimental solar cell characterization results in Section II. Analytical derivations of the insertion loss from adopting a ladder DCR string structures are detailed in Section III. Experimental measurement of the proposed ladder DCR string is presented in Section IV.

II. Photovoltaic Cell Diffusion Capacitance

The commonly used single-diode equivalent circuit model of photovoltaic cells proposed in previous studies is shown in Fig. 1 [21-23]. The *I-V* characteristic of the equivalent solar cell model can be expressed as

$$I_{solar} = I_{SC} - I_d - \frac{V_d}{R_p}. \qquad (1)$$

However, the model in Fig. 1 does not completely capture the dynamics of a solar cell. There is a significant amount of diode capacitance associated with the cell, which is often ignored as a

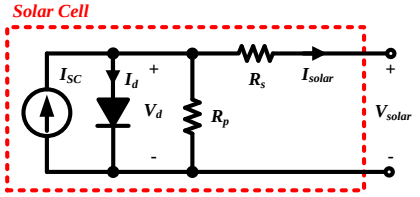

Figure 1. Commonly used single diode solar cell model.

parasitic element when MPPT is considered. The complete equivalent circuit model with a shunt diode capacitance is illustrated in Fig. 2a.

The capacitance of a photovoltaic device is equal to the sum of the diffusion capacitance and the depletion layer capacitance. Since the intended operating solar cell voltage is near the maximum power voltage (V_{mp}), the diffusion capacitance effect dominates and the depletion layer capacitance can be neglected [10]. Diffusion capacitance is the capacitance due to the gradient in charge density inside the cells and is known to have an exponential dependency on the solar cell voltage, or a linear dependency on the solar cell diode current [10-13]. Specifically, the diffusion capacitance C_d can be expressed as

$$C_d = \frac{\tau_F}{V_T} \cdot I_0 \cdot \exp\left(\frac{V_d}{\eta \cdot V_T}\right) = \frac{\tau_F}{V_T} \cdot \left(I_0 + I_d\right) = C_0 + \frac{\tau_F}{V_T} \cdot I_d \ . \quad (2)$$

In Equation (2), V_d is the solar cell diode voltage, I_d is the solar cell diode current, V_T is the thermal voltage, and η is the diode factor. Moreover, I_0 is the dark saturation current of the cell due to diffusion of the minority carriers in the junction, and C_0 is the dark diffusion capacitance. The time constant can be defined as

$$\tau_F^{-1} = \tau^{-1} + \tau_B^{-1}, \quad (3)$$

where τ is the minority carrier lifetime and τ_B is the transit time of the carrier across the diode. If the solar cell base thickness is greater than the minority carrier diffusion length, τ_F can simply be approximated as τ. In general, solar cells made from materials with longer minority carrier lifetimes are more efficient because the light-generated minority carriers persist for a longer time before recombining [24].

A. *Solar Cell Diffusion Capacitance Characterization*

Previous works have revealed that solar cells can exhibit diffusion capacitance in the range of microfarads to hundreds of microfarads near the maximum power point voltage [10,11]. Comparing, for example, to the energy storage capacitance of seven 1µF capacitors used in the resonant switched-capacitor converter in [2], the solar cell itself possesses a sufficient amount of capacitance and offers a great opportunity to drastically limit the number of external passive components. External energy storage capacitors are required in the case of the resonant switched-capacitor converter in [2] because power balancing is applied at the sub-module string level, and the effective capacitance of a sub-module string may not be adequate as it is a series combination of a large number of diffusion capacitors.

Published measurements of cell diffusion capacitance are typically performed by applying a bias voltage across the solar cells, which may not accurately represent the effect of diffusion capacitance in the context of a switched-capacitor converter. Therefore, the switching circuit shown in Fig. 2a is used here to characterize a commercially available mono-crystalline solar cell (P-Maxx-2500mA) as an example. The cell measures 15.6cm-by-6cm, and has an open-circuit voltage of 0.55V and a short-circuit current of 2.5A under maximum lighting conditions. The solar cell capacitance is measured ratiometrically by comparing the charging slopes during the two different phases of operation. The measurement was performed with a switching frequency of 50kHz and repeated over a set of

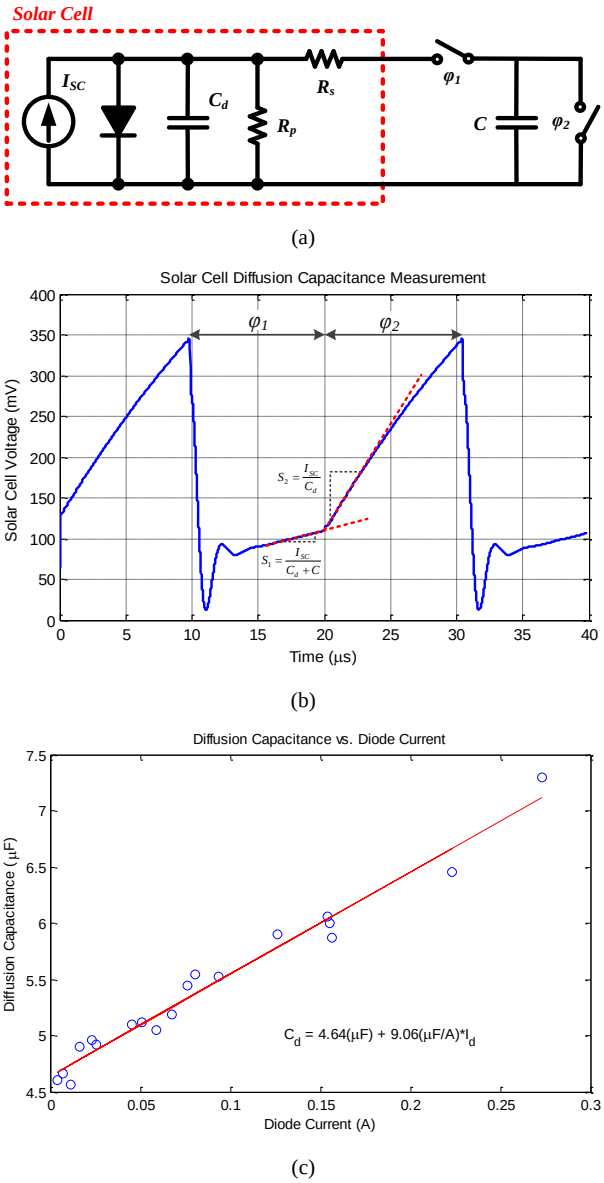

Figure 2. Solar cell capacitance measurement results: (a) characterization switching circuit implementation, (b) switching waveform and (c) capacitance vs. diode current.

known external capacitances between 10µF to 30µF. The corresponding waveforms and the slopes are illustrated in Fig. 2b, and the measured capacitance showing a linear relationship to the solar cell diode current is shown in Fig. 2c.

The measured solar cell has a worst-case, i.e., dark, capacitance of 4.64µF, which matches very well with the measurement result for mono-crystalline solar cells presented in [14]. This minimum capacitance will prove sufficient for DCR power balancing. The relationship between the available capacitance and power conversion loss will be discussed and quantified in Section III. Note that the solar cell diode current is roughly equal to the difference between the short-circuit current and the extracted current. With the typical maximum power current (I_{mp}) being approximately 80-95% of the short-circuit current [1,7], the diode current is 5-20% of the short-circuit current at maximum power point, assuming negligible

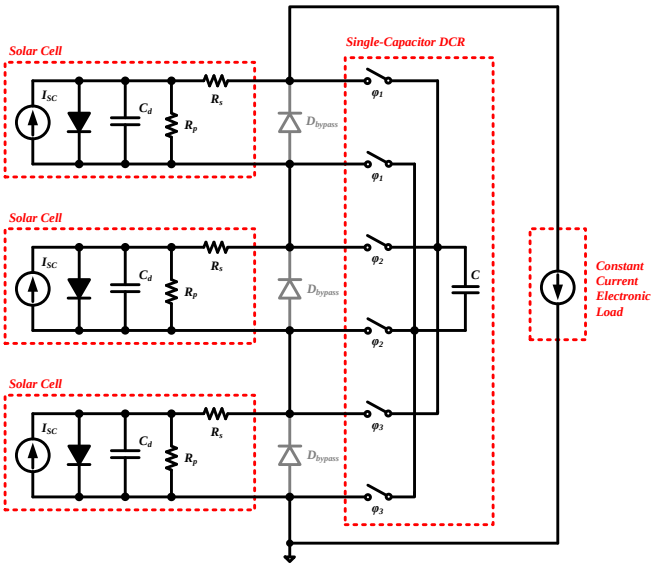

Figure 3. Single-capacitor diffusion charge redistribution validation setup.

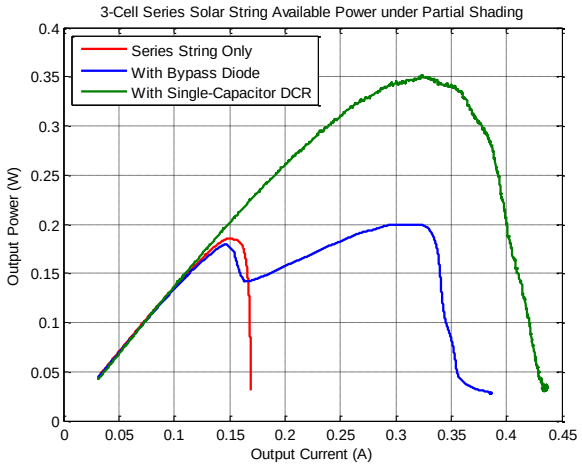

Figure 4. Measured output power vs. output current with and without single-capacitor diffusion charge redistribution.

current through the shunt resistance. Hence, the effective diffusion capacitance for this example cell during normal operation can be as high as 6 to 9µF.

B. Single-Capacitor Diffusion Charge Redistribution

To demonstrate the utility of the solar cell diffusion capacitance as an energy handling component in a power converter, an initial DCR prototype was constructed with a single capacitor. Results from this experiment will lead to a DCR architecture with no external capacitors. The block diagram of this first experimental setup is illustrated in Fig. 3. The prototype consisted of three mono-crystalline solar cells, six IRF9910 MOSFET switches, and a single flying capacitor.

The flying capacitor is connected to each cell sequentially to transfer the imbalance of power among the cells. Since there is no capacitor in parallel with the solar cells to serve as intermediate energy storage when the flying capacitor is disconnected from a cell, the solar cells must therefore rely on their own diffusion capacitance to buffer the different between their respective generated power and extracted power.

By having a single external energy storage element, it can be shown that differential power processing is preserved, and that insertion loss is insignificant. That is, if the cells are well-matched and experience the same irradiance, the cell voltages at maximum power should be identical, resulting in nearly zero net current flow into the flying capacitor and therefore zero loss.

To evaluate the efficacy of the diffusion capacitances in the context of power balancing, a partial shading condition was imposed by covering half of the top cell. In the experiment, the flying capacitor is switched at approximately 300 kHz with a 33% duty cycle for each phase. The output current is swept linearly on an HP 6063B DC Electronic Load at 1A/s and the output voltage and current are measured and recorded. The output power versus output current curve for a series string, a series string with bypass diodes, and a series string with single-capacitor diffusion charge redistribution are shown in Fig. 4.

Under partial shading condition, the series string current is limited by the weakest link, and therefore the extracted power is reduced dramatically. With bypass diode in place, the system can extract additional power from the unshaded cells while bypassing the shaded one; the resulting non-convex output power to current characteristic curve is also illustrated in Fig. 4. Finally, the diffusion capacitances are shown to be very effective in power balancing, extracting significantly more power compared to the series string and the bypassed cases. In addition, a convex output power to current profile is retained, allowing easy integration with existing MPPT-equipped string inverters.

III. Capacitor-less Diffusion Charge Redistribution

It is possible to extend the diffusion charge redistribution scheme to be completely capacitor-less by replacing the flying capacitor with a solar cell and its diffusion capacitance. This enables maximum power point tracking with cell-level granularity without needing any external passive components for energy storage, which translates to the maximum achievable tracking efficiency at the minimum possible cost for power processing. It has been estimated that cell-level maximum-power-point tracking could improve the energy captured in shaded conditions by as high as 30%, a substantial improvement from the estimated 16% with only module-level granularity [15].

The proposed, fully scalable, cell-level power balancing architecture using diffusion charge redistribution is illustrated in Fig. 5. In the proposed topology, a single series string is split into two strings: a load-connected string of N cells in parallel with a switched ladder-connected string of $N-1$ cells used for charge balancing. The load-connected cells are assigned odd designators while the ladder-connected cells are assigned even designators. This approach allows the construction of large series-strings to meet the voltage requirement of a grid-connected inverter, while making the cells appear in pseudo-parallel to mitigate power loss due to mismatch conditions in real-world applications. In short, the switched configuration is able to convert a series-string into an effective single "super-cell".

The reduction in external energy storage does not come without cost – the implicit tradeoff of eliminating all external

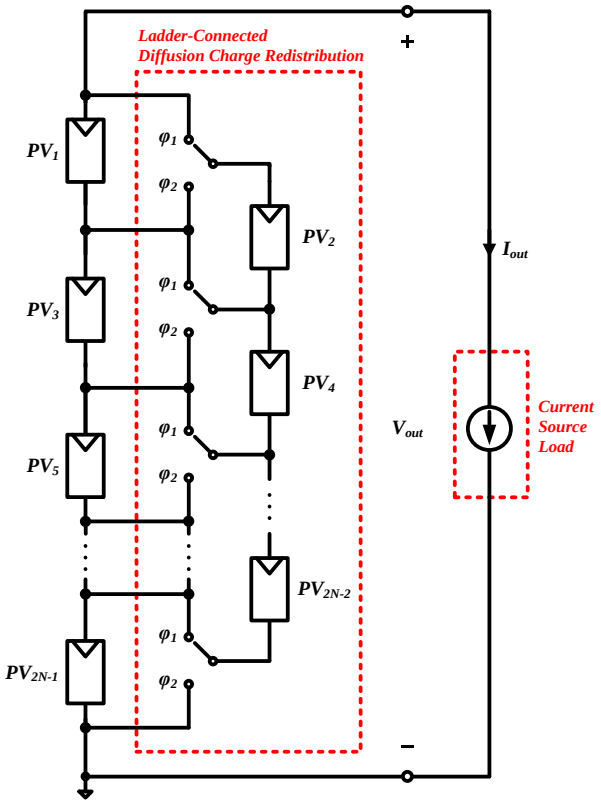

Figure 5. Proposed fully-scalable ladder-connected DCR architecture.

storage is having to process part of the string power, specifically the power generated from the ladder-connected string. In the following section, the power conversion efficiency of such a structure is carefully considered and compared to the traditional series string. The additional power conversion loss incurred from this structure compared to a series string under perfectly matching condition will be characterized as an insertion loss.

The switched-capacitor analysis presented in [16] can be generalized to distributed power generation for calculating the insertion loss of adopting diffusion charge redistribution. The switched-capacitor conversion loss can be characterized by two asymptotic limits: the slow- and fast-switching limits. In the slow-switching limit (SSL), the output impedance of the switching converter is calculated assuming all switches and interconnects are ideal, and the capacitors experience impulses of current. In the fast-switching limit (FSL), the capacitor voltages are assumed to be constant, and the switch and interconnect resistances dominate the losses. After deriving both the SSL and FSL losses, the total switched-capacitor loss can be computed as a combination of the slow-switching and fast-switching limit losses.

A. *Slow-Switching Limit Power Conversion Loss*

For illustration, the SSL insertion loss calculation is performed on a 3-2 example string, where N is equal to 3 following the convention shown in Fig. 5. The charge flow diagram of the 3-2 example string in the two phases are illustrated in Fig. 6. The charge flow is designated as $q^{\varphi}_{x,i}$, where x describes the element, i represents the index number, and φ denotes the phase. For example, $q^{1}_{pv,2}$ corresponds to the total

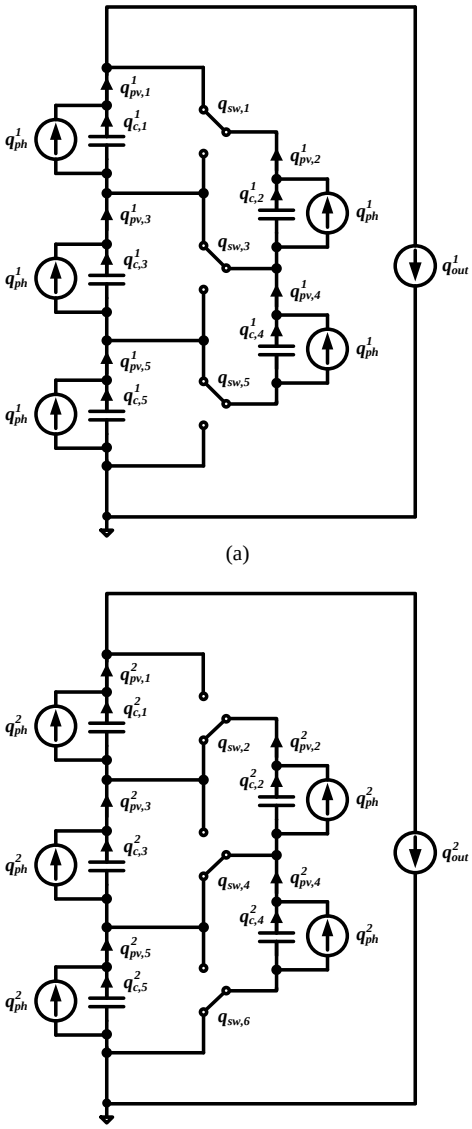

Figure 6. Charge flow in proposed cell-level power balancing architecture using a 3-2 ladder DCR string configuration. (a) phase 1 (b) phase 2.

charge extracted from the second photovoltaic element during phase 1. For the insertion loss calculation, it is assumed that the solar cells are perfectly matched and each cell contains a constant photo-current source generating a total charge of q_{ph} over a complete switching period. For a photo-current source in this two-phase converter,

$$q^{1}_{ph} = q^{2}_{ph} = q_{ph}/2 . \tag{4}$$

The output is represented by a constant current load drawing a total charge of q_{out} over a complete switching period. That is, q_{out} is the sum of the output charges delivered during phase 1 and phase 2, and therefore

$$q^{1}_{out} = q^{2}_{out} = q_{out}/2 . \tag{5}$$

By using capacitor charge balance in steady state, we can write

$$q^{1}_{pv,i} + q^{2}_{pv,i} = q_{ph} , \tag{6}$$

for $i = [1, 2, \ldots, 5]$. By Kirchhoff's current law (KCL), we can further write (7) and (8) for the two phases.

$$q^1_{pv,1} + q^1_{pv,2} = q^1_{pv,3} + q^1_{pv,4} = q^1_{pv,5} = q_{out}/2 \tag{7}$$

$$q^2_{pv,1} = q^2_{pv,2} + q^2_{pv,3} = q^2_{pv,4} + q^2_{pv,5} = q_{out}/2 \tag{8}$$

Solving this system of equations (6), (7) and (8) iteratively yields the relationship between the photo-current from each cell and the string output current, as shown in (9).

$$q_{out} = \frac{5}{3} \cdot q_{ph} \tag{9}$$

Each charge flow can then be expressed in terms of the output charge over a complete switching period. Following the convention in [16], the normalized charge flow, or the charge multiplier will be defined as:

$$a^{\varphi}_{x,i} = \frac{q^{\varphi}_{x,i}}{q_{out}}. \tag{10}$$

The SSL charge multiplier of each photovoltaic cell in the 3-2 DCR string during the two phases is summarized in Table I.

The net charge flowing into any diffusion capacitance over a complete switching cycle in steady state will be zero. Each capacitor in Fig. 6 will experience an equal but opposite charge delivery during the two phases. The magnitude of the charge flows for the capacitors can therefore be expressed as the difference between the charge extracted from the solar cell, and the charge generated by the photo-current source within the cell during either phase.

$$a_{c,i} = \frac{|q_{c,i}|}{q_{out}} = \frac{|q^{\varphi}_{pv,i} - q_{ph}/2|}{q_{out}} \tag{11}$$

Equation (11) can be used to determine the SSL charge multipliers of the capacitors, which are summarized in Table II.

The capacitor charge multiplier vector can be generalized to a DCR string with $2N-1$ cells, where there are N cells in the load-connected string and $N-1$ cells in the ladder-connected string. In the general case, the output current to photocurrent ratio and the capacitor charge multiplier expressions are shown in (12) and (13) respectively.

$$q_{out} = \frac{2N-1}{N} \cdot q_{ph} \tag{12}$$

$$a_{c,i} = \frac{|q_{c,i}|}{q_{out}} = \frac{|N-i|}{4N-2} \tag{13}$$

The SSL output impedance [16] of the DCR string can then be written as

$$R_{SSL} = \sum_{i=1}^{2N-1} \frac{(a_{c,i})^2}{C_d \cdot f_{sw}} = \frac{1}{12} \cdot \frac{N \cdot (N-1)}{2N-1} \cdot \frac{1}{C_d \cdot f_{sw}}. \tag{14}$$

In order to calculate percentage insertion loss, the ratio of the SSL output impedance to the load resistance must be calculated. This can be found as an expression in terms of the performance of each cell in steady state, operating at its maximum power point with voltage V_{mp} and current I_{mp}. Using (12), which effectively relates cell current to output current, and the fact that the DCR string voltage equals N times the cell voltage as shown in Fig. 5, the load resistance is

$$R_L = \frac{V_{out}}{I_{out}} = \frac{N \cdot V_{mp}}{\frac{2N-1}{N} \cdot I_{mp}} = \frac{N^2}{2N-1} \cdot \frac{V_{mp}}{I_{mp}}. \tag{15}$$

The insertion loss fraction, IL_{SSL} can be calculated as the ratio of the SSL output impedance of the DCR string to the load resistance,

$$IL_{SSL} = \frac{R_{SSL}}{R_L} = \frac{1}{12} \cdot \frac{N-1}{N} \cdot \frac{1}{f_{sw}} \cdot \frac{1}{V_{mp}} \cdot \frac{I_{mp}}{C_d}, \tag{16}$$

and the SSL efficiency of the array can be defined as one minus the SSL insertion loss. Equation (16) represents a fundamental result that is dependent on technology and material choices. It states that the SSL efficiency of a solar array configured as a DCR string is effectively dictated by the ratio of the maximum power current to the diffusion capacitance, for large N. For illustration, assume the following rounded numbers for our solar cells under maximum illumination: a maximum power voltage of 0.5V, a maximum power current of 2A, and a diffusion capacitance of 9µF. For a DCR string with N of 20 and a switching frequency of 1MHz, the insertion loss can be calculated to be a manageable 3.5%.

The SSL insertion loss is not the only loss mechanism. It is possible for the DCR string to operate near the SSL-FSL transition where the loss contributions are approximately equal, or deep in FSL where the FSL losses dominate. Hence, to complete the system-level insertion loss characterization, the string output characteristics in the fast-switching limit is considered in the next section.

TABLE I. SSL PV CELL CHARGE MULTIPLIER FOR 3-2 DCR STRING

Phase (φ)	**SSL PV Cell Charge Multiplier**				
	$a^{\varphi}_{pv,1}$	$a^{\varphi}_{pv,2}$	$a^{\varphi}_{pv,3}$	$a^{\varphi}_{pv,4}$	$a^{\varphi}_{pv,5}$
1	1/10	4/10	3/10	2/10	5/10
2	5/10	2/10	3/10	4/10	1/10

TABLE II. SSL CAPACITOR CHARGE MULTIPLIER FOR 3-2 DCR STRING

SSL Capacitor Charge Multiplier				
$a_{c,1}$	$a_{c,2}$	$a_{c,3}$	$a_{c,4}$	$a_{c,5}$
2/10	1/10	0	1/10	2/10

TABLE III. FSL SWITCH CHARGE MULTIPLIER FOR 3-2 DCR STRING

FSL Switch Charge Multiplier					
$a_{sw,1}$	$a_{sw,2}$	$a_{sw,3}$	$a_{sw,4}$	$a_{sw,5}$	$a_{sw,6}$
4/10	2/10	2/10	2/10	2/10	4/10

B. Fast-Switching Limit Power Conversion Loss

In the fast-switching limit (FSL), the capacitor voltages are assumed to be constant during a switching period. In addition, the duty cycle becomes an important consideration [16]. For the following analysis, a 50% duty cycle is assumed for simplicity. The output impedance will again be derived in the context of

the 3-2 DCR example string for illustration, then generalized to a DCR string of arbitrary size.

From Fig. 6, the charge flowing through the switches can be written using the PV cell charge multipliers as shown in (17).

$$a_{sw,i} = \begin{cases} \left| a^1_{pv,i+1} - a^1_{pv,i-1} \right| & , \quad i \text{ odd} \\ \left| a^2_{pv,i} - a^2_{pv,i-2} \right| & , \quad i \text{ even} \end{cases} \tag{17}$$

where boundary cases, i.e., $a^1_{pv,0}$ and $a^2_{pv,2N}$ are assumed to be zero. The resulting FSL charge multiplier vector for the 3-2 DCR string is summarized in Table III. For a DCR string with $2N-1$ total cells, the FSL switch charge multiplier vector can be derived as

$$a_{sw,i} = \begin{cases} (N-1)/(2N-1) & , \quad i = 1, 2N \\ 1/(2N-1) & , \quad \text{otherwise} \end{cases}. \tag{18}$$

Hence, the FSL output impedance of an arbitrarily sized DCR string is

$$R_{FSL} = 2 \cdot \sum_{i=1}^{2N-1} R_{eff} \cdot (a_{sw,i})^2 = 4 \cdot \frac{N \cdot (N-1)}{(2N-1)^2} \cdot R_{eff}, \tag{19}$$

where R_{eff} is the effective resistance of the switch on-resistance in series with any interconnect resistance. Relating the FSL output impedance back to the load resistance, the FSL percentage insertion loss can be calculated as

$$IL_{FSL} = \frac{R_{FSL}}{R_L} = \frac{4}{2N-1} \cdot \frac{N-1}{N} \cdot \frac{I_{mp}}{V_{mp}} \cdot R_{eff}. \tag{20}$$

The result in (20) makes intuitive sense because the loss from the fast-switching limit is expected to be inversely proportional to the number of cells behaving like current sources. The dissipated power in the switches is approximately constant for sufficiently large *N*, while the total generated power increases linearly with *N*. Note that the factor of 4 in (20) can be derived by using the fact that the power extracted from the ladder-connected string must pass through two switching devices. In addition, the current through the switches resemble a square wave, which gives an additional factor of two in power.

From (20), the FSL insertion loss, or conduction loss, can almost always be made negligible for a sufficiently large string. For example, for a DCR string with *N* of 20, maximum power current of 2A, maximum power voltage of 0.5V, and an effective switch on-resistance of 15mΩ, the FSL insertion loss is only 0.58%.

The total insertion loss can be calculated by combining the SSL and FSL losses. A conservative approximation, the root of the quadratic sum the two loss components, will be used for the remainder of this paper. That is,

$$IL_{TOT} \cong \sqrt{(IL_{SSL})^2 + (IL_{FSL})^2}. \tag{21}$$

C. Recovered Power Loss from Process Variation

The DCR power processing approach also effectively corrects for process variation between cells, which normally would limit power extraction from a string of cells. DCR, therefore, can improve power extraction from an array of mismatched cells in comparison to other approaches for processing power. Alternatively, DCR can be viewed as easing the manufacturing problem of assembling a solar array by accommodating greater cell variation while maximizing power extraction.

Process variation in photovoltaic manufacturing typically refers to the *I-V* mismatch between the solar cells. For a series string of solar cells, *I-V* mismatch can negatively impact the overall tracking efficiency because the cells may not operate at their individual maximum power points. Instead, they operate at a collective maximum power current for all the cells present in the series string.

In order to improve the cell-level tracking efficiency by reducing cell-to-cell variation, solar panel manufacturers have invested greatly in improving their manufacturing process as well as evaluating different cell binning algorithms [17,18]. In the past ten years, the manufacturers have been able to refine their production process and reduce the power tolerance from ±10% down to ±3% [19]. Nevertheless, the *I-V* mismatch can still have higher tolerance when cells are sorted by maximum power.

The subsequent analysis follows [8] in using a first-order approximation for cell output power under deviation from the maximum power point operation. Assuming approximately constant voltage near the maximum power point, the output power (P_{cell}) can be assumed to be step-wise linear when the cell output current (I_{cell}) is slightly perturbed around the maximum power current:

$$I_{cell} = (1-\delta) \cdot I_{mp} \tag{22}$$

$$P_{cell} = (1-|\delta|) \cdot P_{mp} \tag{23}$$

To understand the effect of variation on a string, let δ_i be a random variable which describes the deviation of the current at the collective maximum power of the string to the current of cell *i* at its maximum power operation. That is, the total power from a series string can be written as

$$P_{string} = \sum_i (1-|\delta_i|) \cdot P_{mp} \tag{24}$$

Then the expected power from a series string of *N* cells can be expressed as

$$E[P_{string}] = N \cdot P_{mp} \cdot (1 - E[|\delta|]) \tag{25}$$

Using (25), the power loss due to process variation can be approximated as the deviation from the maximum available string power $N \cdot P_{mp}$. This represents a conservative estimate; the actual power loss can be higher because the magnitude of *dP/dI* can be much higher when $I > I_{mp}$. For a more detailed treatment, a Monte Carlo analysis of the expected power with cell-to-cell variation can be found in [8].

Assuming a uniform distribution of δ_i with a range of ±5%, the loss in tracking efficiency in a series string due to process variation is approximately 2.5%. Since the DCR string is able to mitigate even larger partial shading mismatches, it will be practically indifferent to the asymmetry from process variation. Hence, the loss in tracking efficiency from cell-to-cell variation, illustrated by $E[|\delta|]$ in (25), can be naturally recovered. A correction factor is introduced in the overall insertion loss calculation, and complete insertion loss from using a DCR string can then be approximated as

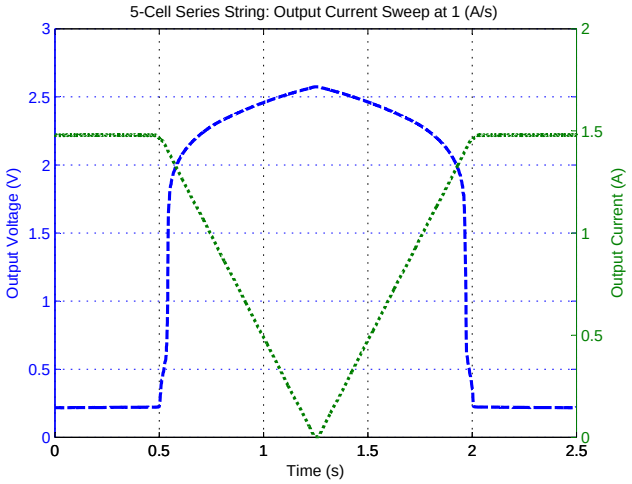

Figure 7. Experimental measurement of output voltage and current of a 5-cell series string by sweeping the output current at 1 ampere per second.

$$\mathit{IL}_{DCR} \cong \sqrt{(\mathit{IL}_{SSL})^2 + (\mathit{IL}_{FSL})^2} - E[|\,\delta\,|]. \qquad (26)$$

Potentially the greatest value in performing cell-level MPPT with diffusion charge redistribution lies in the fact that the string output power becomes independent of cell-to-cell process variation. Therefore, it is possible to drastically reduce manufacturing cost by relaxing the extensive and stringent binning process currently employed in manufacturing. It may also greatly simplify manufacturing and assembly processes.

IV. Experimental Validation

A 5-cell series string and a 3-2 DCR string experimental prototypes were constructed to further validate the proposed concept. The DCR prototype consisted of five P-Maxx-2500mA mono-crystalline solar cells, six IRF9910 MOSFET switches, and five LSM115J Schottky diodes. The characteristic output power versus output current curve is obtained by recording both the string output voltage and the output current as an HP 6063B DC Electronic Load sweeps the output current from 0-10A at a slew rate of 1 ampere per second.

As the electronic load demands more current than the series string can supply, the current saturates at the short-circuit current of the string, as illustrated in Fig. 7. Furthermore, the effect of process variation can be observed in the voltage waveform. That is, if the short-circuit current of the individual cells are perfectly matched, the string is expected to have a zero output voltage at the short-circuit current. However, if there is mismatch between the cells, cells with higher short-circuit circuit can maintain a positive voltage as the string current is limited by the cells with lower short-circuit current.

Figure 8 shows the experimental output power measurement of a 5-cell series string with and without bypass diodes, compared to a 3-2 DCR string. From the 5-cell series string measurement under uniform irradiance in Fig. 8a, the maximum power current I_{mp} and voltage V_{mp} of the cells can be extracted to be 1.31A and 0.40V respectively. The diffusion capacitance can then be calculated from Fig. 2c to be approximately 6.25μF. The DCR string has a switching frequency of 500kHz, and the expected SSL conversion loss is 5.8% from (16). Assuming the

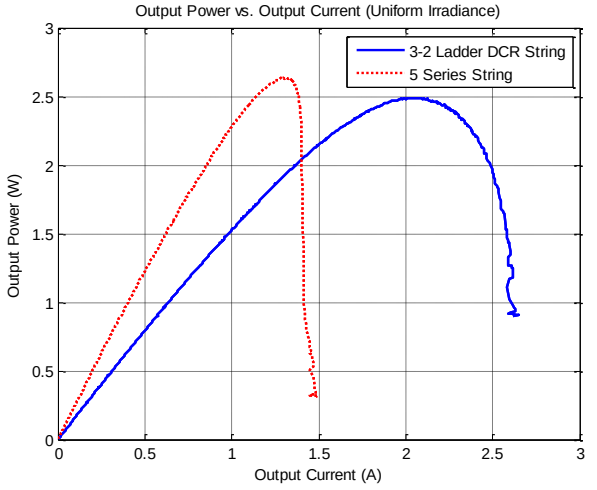

(a)

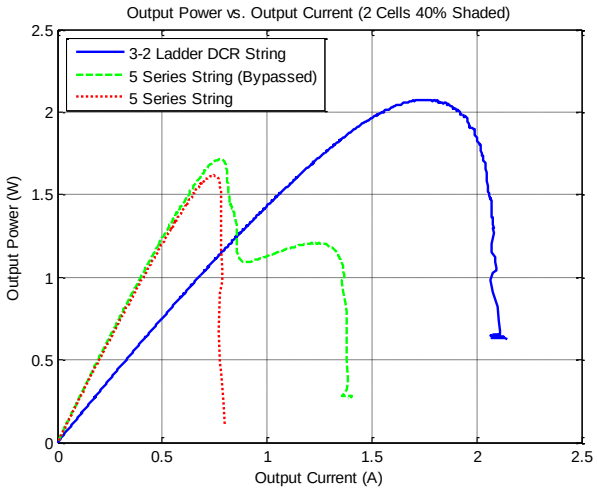

(b)

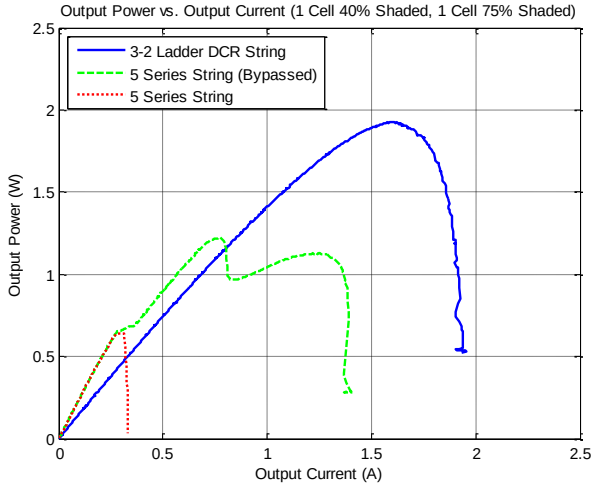

(c)

Figure 8. Experimental measurement of a 3-2 DCR string under various partial shading conditions compared to the 5 series string. (a) uniform irradiance (b) 2 cells 40% shaded, (c) 1 cell 40% shaded and 1 cell 75% shaded.

TABLE IV. MEASURED OUTPUT POWER COMPARISON AND EFFICIENCY SUMMARY

Configuration (N = 3)	**Uniform Irradiance**		**2 Cells 40% Shaded (16% Overall Shading)**		**1 Cell 40% Shaded, 1 Cell 75% Shaded (23% Overall Shading)**	
	Power (W)	*Conversion Efficiency*	*Power (W)*	*Extracted Percentage*	*Power (W)*	*Extracted Percentage*
Series String	2.63	100%	1.62	61.6%	0.64	24.3%
Series + Bypass	2.63	100%	1.71	65.0%	1.22	46.4%
DCR String	2.49	94.7%	2.075	83.3%	1.92	77.1%

switch on-resistance dominates the effective resistance, the expected FSL conversion loss is 4.1% from (20). Hence, the total insertion loss can be calculated from (21) to be 7.1%.

The measured output power of the 5-cell series string has a peak at 2.63W, and the measured output power of the 3-2 DCR string has a maximum of 2.49W. This gives a measured efficiency of 94.7%, or a measured DCR insertion loss of 5.3%. The lower measured insertion loss, compared to the calculated 7.1%, can be attributed to the recovery of losses from process variation as shown in (26).

Figures 8b and 8c illustrate the measured output power characteristic curves under different shading conditions, where the shading percentage is determined by measuring the change in short-circuit current of the shaded cells. The series string is shown to lose a significant portion of the string power even when only a small percentage of the total area is shaded. With bypass diodes in place, the string is able to extract more power. However, the resulting output power characteristic curve is non-convex, i.e., with multiple maxima, which introduces additional constraints to the required MPPT algorithm. In the case of the DCR string, significantly more power can be extracted. Moreover, the output power characteristic curve remains convex, which greatly reduces the complexity of the required MPPT algorithm.

The maximum measured power for each configuration is tabulated in Table IV, where the extracted percentage column illustrates the ratio of power extracted to the total available power under uniform irradiance for the same configuration. It can be seen that in the case of DCR, the extracted percentage follows one minus the overall shading percentage quite closely, which validates the effectiveness of the proposed power balancing technique.

V. CONCLUSION

A new cell-level power balancing scheme, *diffusion charge redistribution*, has been presented to increase energy extraction and improve maximum power point tracking efficiency under partial shading conditions. This technique makes an array of solar cells behave as an effective single super-cell, which can also potentially eliminate the need for testing and binning during production and thereby reduce manufacturing cost. The proposed technique trades off processing power differentially to minimizing the number of external energy storage components. In the limit where only the intrinsic solar cell diffusion capacitances are used for cell-level power balancing, the finest achievable MPPT granularity can be reached at the minimum possible cost for power electronics.

A fully-scalable ladder-type DCR string architecture has been presented along with the analysis method to characterize the insertion losses at the slow-switching and fast-switching limits. A proof-of-concept system consisting of a 3-2 DCR string has been constructed and characterized. Experimental results show the DCR string extracting significantly more energy under various partial shading conditions compared to its series string counterparts.

ACKNOWLEDGMENT

The authors gratefully acknowledge the support of The Grainger Foundation and the Kuwait-MIT Program.

REFERENCES

[1] Olalla, C.; Rodriguez, M.; Clement, D.; Jian Wang; Maksimovic, D., "Architecture and control of PV modules with submodule integrated converters," *Control and Modeling for Power Electronics (COMPEL), 2012 IEEE 13th Workshop on* , vol., no., pp.1,6, 10-13 June 2012

[2] Stauth, J.T.; Seeman, M.D.; Kesarwani, K., "A Resonant Switched-Capacitor IC and Embedded System for Sub-Module Photovoltaic Power Management," *Solid-State Circuits, IEEE Journal of* , vol.47, no.12, pp.3043,3054, Dec. 2012

[3] Stauth, J.T.; Seeman, M.D.; Kesarwani, K., "Resonant Switched-Capacitor Converters for Sub-module Distributed Photovoltaic Power Management," *Power Electronics, IEEE Transactions on* , vol.28, no.3, pp.1189,1198, March 2013

[4] Shenoy, P.S.; Kim, K.A.; Krein, P.T., "Comparative analysis of differential power conversion architectures and controls for solar photovoltaics," *Control and Modeling for Power Electronics (COMPEL), 2012 IEEE 13th Workshop on* , vol., no., pp.1,7, 10-13 June 2012

[5] Shenoy, P.S.; Kim, K.A.; Johnson, B.B.; Krein, P.T., "Differential Power Processing for Increased Energy Production and Reliability of Photovoltaic Systems," *Power Electronics, IEEE Transactions on* , vol.28, no.6, pp.2968,2979, June 2013

[6] Qin, Shibin; Pilawa-Podgurski, Robert C.N., "Sub-module differential power processing for photovoltaic applications," *Applied Power Electronics Conference and Exposition (APEC), 2013 Twenty-Eighth Annual IEEE* , vol., no., pp.101,108, 17-21 March 2013

[7] Walker, G.R.; Sernia, P.C., "Cascaded DC-DC converter connection of photovoltaic modules," *Power Electronics Specialists Conference, 2002. pesc 02. 2002 IEEE 33rd Annual* , vol.1, no., pp.24,29 vol.1, 2002

[8] Chang, A.H.; Cooley, J.J.; Leeb, S.B., "A systems approach to photovoltaic energy extraction," *Applied Power Electronics Conference and Exposition (APEC), 2012 Twenty-Seventh Annual IEEE* , vol., no., pp.59,70, 5-9 Feb. 2012

[9] Trubitsyn, A.; Pierquet, B.J.; Hayman, A.K.; Gamache, G.E.; Sullivan, C.R.; Perreault, D.J., "High-efficiency inverter for photovoltaic applications," *Energy Conversion Congress and Exposition (ECCE), 2010 IEEE* , vol., no., pp.2803,2810, 12-16 Sept. 2010

[10] G. Friesen, H.A. Ossenbrink, "Capacitance effects in high-efficiency cells," *Solar Energy Materials and Solar Cells*, Volume 48, Issues 1–4, November 1997, Pages 77-83

[11] S.K. Sharma, D. Pavithra, G. Sivakumar, N. Srinivasamurthy, B.L. Agrawal, "Determination of solar cell diffusion capacitance and its dependence on temperature and 1 MeV electron fluence level," *Solar Energy Materials and Solar Cells*, Volume 26, Issue 3, April 1992, Pages 169-179

[12] R. Anil Kumar, M.S. Suresh, J. Nagaraju, "Measurement and comparison of AC parameters of silicon (BSR and BSFR) and gallium arsenide (GaAs/Ge) solar cells used in space applications," *Solar Energy Materials and Solar Cells*, Volume 60, Issue 2, 15 January 2000, Pages 155-166

[13] R.Anil Kumar, M.S. Suresh, J. Nagaraju, "Silicon (BSFR) solar cell AC parameters at different temperatures," *Solar Energy Materials and Solar Cells*, Volume 85, Issue 3, 31 January 2005, Pages 397-406

[14] Jeevandoss, C. R.; Kumaravel, M.; Kumar, V.J., "A novel method for the measurement of the C-V characteristic of a solar photovoltaic cell," *Instrumentation and Measurement Technology Conference (I2MTC)*, 2010 IEEE , vol., no., pp.371,374, 3-6 May 2010

[15] MacAlpine, S.M.; Erickson, R.W.; Brandemuehl, M.J., "Characterization of Power Optimizer Potential to Increase Energy Capture in Photovoltaic Systems Operating Under Nonuniform Conditions," *Power Electronics, IEEE Transactions on* , vol.28, no.6, pp.2936,2945, June 2013

[16] Seeman, M.D.; Sanders, S.R., "Analysis and Optimization of Switched-Capacitor DC-DC Converters," *Computers in Power Electronics, 2006. COMPEL '06. IEEE Workshops on* , vol., no., pp.216,224, 16-19 July 2006

[17] Field, H.; Gabor, A.M.; , "Cell binning method analysis to minimize mismatch losses and performance variation in Si-based modules," *Photovoltaic Specialists Conference, 2002. Conference Record of the Twenty-Ninth IEEE* , vol., no., pp. 418- 421, 19-24 May 2002

[18] Karen Wilson; Denis De Ceuster; Ronald A. Sinton; , "Measuring the Effect of Cell Mismatch on Module Output," *Photovoltaic Energy Conversion, Conference Record of the 2006 IEEE 4th World Conference on* , vol.1, no., pp.916-919, May 2006

[19] Noguchi, T.; Togashi, S.; Nakamoto, R.; , "Short-current pulse based adaptive maximum-power-point tracking for photovoltaic power generation system," *Industrial Electronics, 2000. ISIE 2000. Proceedings of the 2000 IEEE International Symposium on* , vol.1, no., pp.157-162 vol.1, 2000

[20] Romero-Cadaval, E.; Spagnuolo, G.; Garcia Franquelo, L.; Ramos-Paja, C.A.; Suntio, T.; Xiao, W.M., "Grid-Connected Photovoltaic Generation Plants: Components and Operation," *Industrial Electronics Magazine, IEEE* , vol.7, no.3, pp.6,20, Sept. 2013

[21] R. F. Coelho, F. Concer, and D. C. Martins, "A proposed photovoltaic module and array mathematical modeling destined to simulation," *in Proc. IEEE Int. Symp. Industrial Electronics*, 2009, pp. 1624–162.

[22] A. Chatterjee, A. Keyhani, and D. Kapoor, "Identification of photovoltaic source models," *IEEE Trans. Energy Convers*., vol. 26, no. 3, pp. 883–889, Sept. 2011.

[23] M. G. Villalva, J. R. Gazoli, and E. R. Filho, "Comprehensive approach to modeling and simulation of photovoltaic arrays," *IEEE Trans. Power Electron.*, vol. 24, no. 5, pp. 1198–1208, May 2009.

[24] R. Jayakrishnan, Shreyans Gandhi, Prakash Suratkar, "Correlation between solar cell efficiency and minority carrier lifetime for batch processed multicrystalline Si wafers," *Materials Science in Semiconductor Processing*, Volume 14, Issues 3–4, September–December 2011, Pages 223-228.

[25] Seeman, M.D.; "A Design Methodology for Switched-Capacitor DC-DC Converters," Ph.D. dissertation, Dept. EECS, University of California, Berkeley, May, 2009.